Available online at www.sciencedirect.com
ScienceDirect
International Journal of Machine Tools & Manufacture 46 (2006) 1996–2008
INTERNATIONAL JOURNAL OF MACHINE TOOLS & MANUFACTURE DESIGN, RESEARCH AND APPLICATION
www.elsevier.com/locate/ijmactool

Sub-nanosecond monitoring of micro-hole electrical discharge machining pulses and modeling of discharge ringing

C.C. Kao, Albert J. Shih*

Department of Mechanical Engineering, University of Michigan, Ann Arbor, MI 48109, USA

Received 31 October 2005; received in revised form 22 December 2005; accepted 9 January 2006
Available online 3 March 2006

Abstract

Monitoring the gap voltage and current in micro-hole electrical discharge machining (EDM) using high-speed data acquisition with 0.5 ns sampling period is conducted. The spark and arc pulses at three stages, namely electrode dressing, drilling, and penetration, of the micro-hole EDM are recorded. The EDM process parameters are setup to use negative polarity to blunt the electrode tip and positive polarity for micro-hole drilling and penetration. A new phenomenon of pre-discharging current is discovered. In the first 20–30 ns of spark and arc pulses, the current starts to rise while the voltage remains the same. Effects of EDM process parameters, including the open voltage, electrode diameter, and polarity, on the rate of spark and arc pulses and electrode feed rate are investigated. A model based on the RLC circuit is developed to study the ringing effect at the end of a discharge. The intrinsic parasitic capacitance and resistance of a RLC circuit are calculated from the decaying voltage signal and compared under two sets of experiments with varying wire electrode diameter and gap voltage to validate the ringing model. The calculation and experimental results validate the proposed RLC model for ringing phenomenon. The model shows the electrode diameter has negligible effect on ringing and high open voltage increases the parasitic resistance and damping in ringing. The monitoring technique and ringing model developed in this research can assist in the selection and optimization of micro-hole EDM process parameters.

Keywords: Micro-hole EDM; Monitoring; Electrode wear; Ringing effect

1. Introduction

Electrical discharge machining (EDM) is a process widely used in industry to generate micro-holes in hard, electrically conductive work-materials [1,2]. One of the leading applications of micro-hole EDM is the machining of diesel engine fuel injector spray holes [3,4]. The diesel fuel is injected from an array of micro-holes at the tip of an injector under high pressure, atomized into small droplets, and ignited to produce the combustion energy. The EDM of precision spray holes with consistent size, flow rate, and orientation is crucial to the clean combustion of diesel engines, required for meeting the tightening emission regulations for nitrogen oxide (NO_x) and particulate matter [5]. In the past few years, to enhance the atomization of diesel fuel during injection and to achieve homogeneous charge compression ignition (HCCI) [6], a trend of reducing the diameter of spray holes has been identified in diesel engine injector design. The technical challenge in manufacturing is to develop a robust and efficient micro-hole EDM process. Monitoring of EDM pulses using high-speed data acquisition is an essential part of the EDM process control and optimization.

A wire electrode, as illustrated in Fig. 1, is used in micro-hole EDM to penetrate the workpiece and generate a micro-hole. The wire electrode is supported by a wire guide, usually made of ceramic, and fed by a servo motion control system along the wire axial direction. Sparks are generated near the tip of the wire electrode to erode and remove the work material. Tungsten is the most common electrode material because of its high melting temperature (3370 °C) and low tool wear rate. The tungsten wire electrode is centerless ground [7] to achieve uniform size and can be as small as 30 μm in diameter. A scanning electron microscopy (SEM) micrograph of the 0.15 mm diameter injector micro-hole is shown in Fig. 2.

*Corresponding author. Tel.: +1 734 647 1766; fax: +1 734 936 0363.
E-mail address: shiha@umich.edu (A.J. Shih).

0890-6955/$ - see front matter © 2006 Elsevier Ltd. All rights reserved.
doi:10.1016/j.ijmachtools.2006.01.008

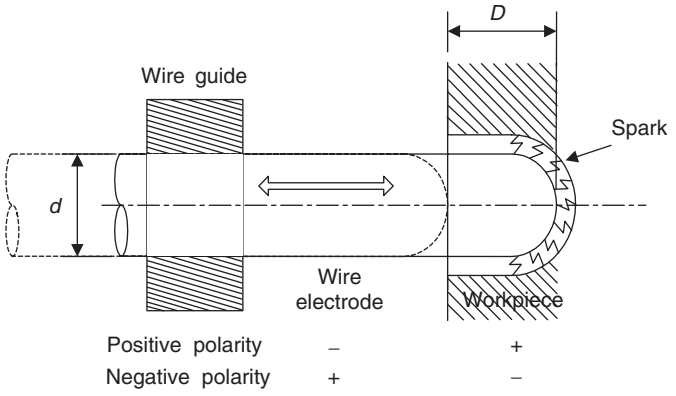

Fig. 1. Schematic diagram of micro-hole EDM and the definition of polarity and drilling depth (D).

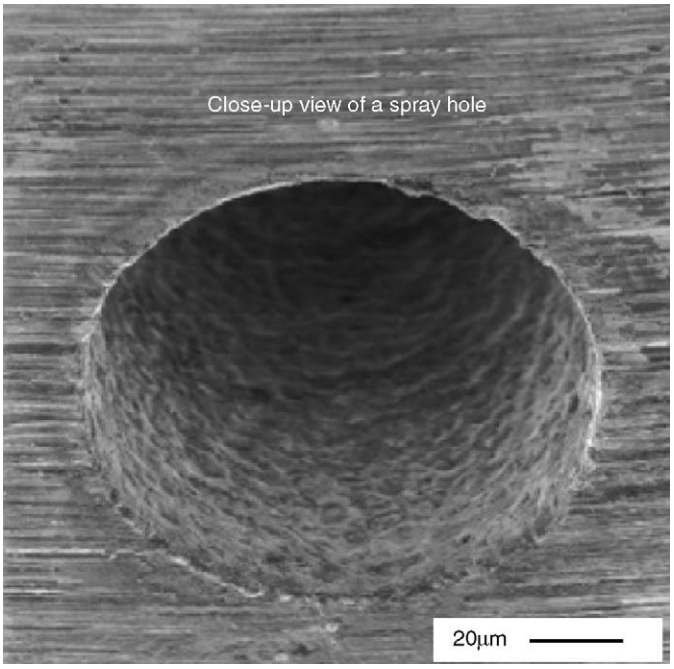

Fig. 2. An SEM micrograph of a diesel engine injector spray hole.

EDM has a slow material removal rate (MRR). In micro-hole EDM, the MRR is further limited due to the narrow gap between electrode and workpiece for debris flushing. The voltage and current across the gap between the electrode and workpiece greatly influence the MRR in micro-hole EDM. To enable efficient MRR in micro-hole EDM, very short (less than 1 μs) pulse duration and high (above 200 V) open circuit voltage, as compared with conventional wire and die-sinking EDM, are typically utilized. The high pulse rate in micro-hole EDM requires a high-speed data acquisition system to record the rapid change of gap voltage and current. In this study, an oscilloscope with 2 GHz sampling rate (0.5 ns sampling period) is utilized for EDM process monitoring.

The efficiency and quality of EDM drilling can be improved with the rotation of electrodes [8–10]. But for micro-hole EDM for fuel injector spray holes, to achieve the required hole dimensional and form accuracy and the stringent flow rate specification, the rotation of the thin, 100–150 μm diameter, electrode is not desirable. Because the electrode extends 2–3 mm from the wire guide, the rotation of electrode will introduce excessive error motion at the electrode tip and cause inconsistency in the micro-hole EDM drilling for diesel engine spray hole applications. Stationary electrode without rotation is investigated in this study.

At the end of discharging, due to the parasitic inductance and inherent capacitance of the EDM circuit, the voltage does not immediately reduce to the steady-state value. This has been recognized as the so-called ringing effect [11], as illustrated in Fig. 3. The ringing effect is an unavoidable phenomenon in EDM. For micro-hole EDM, the ringing effect is significant. The voltage oscillates for a long period of time after the discharging and slowly reduces to a steady-state value. Shortening the time duration of ringing could lead to more frequent EDM pulses and higher MRR. To better understand the ringing effect, a model of the EDM circuit at the discharge stage is necessary. The RC circuit [2,12] and field effect transistor (FET) circuit [13] have been proposed to model the EDM discharging. However, these models are not applicable to studying the ringing effect. A new model based on an expanded serial RLC circuit in a linear rail gun proposed by Kuo et al. [11] is developed. In this study, a model based on a RLC circuit including the inductance effect of the wire electrode and voltage probe jumper cable, was proposed.

Another phenomenon in micro-hole EDM is the current flowing in the opposite direction near the end of EDM pulse. The parasitic components induce a reverse current [3], which can lead to inferior surface roughness and excessive electrode wear [7,8]. The reverse current is also observed in both spark and arc pulses during this micro-hole EDM study.

In this paper, the experimental setup and monitoring procedures are first introduced. Characterization of spark, arc, and short pulses in three stages during micro-EDM is discussed. The pulse rate and electrode feed rate are investigated. Finally, the RLC model of the ringing effect in micro-hole EDM is presented.

2. Experimental setup and monitoring procedures

2.1. Micro-hole EDM machine

Experiments were conducted in a micro-hole EDM machine, Ann Arbor Machine Model 1S15. Tungsten wire electrodes with 100, 125, and 225 μm diameter were used to drill micro-holes. The spark, arc, and short pulses were recorded. To develop and validate the discharge-ringing model, the open circuit voltage was set at 160, 180, 200, 230, and 250 V using the 125 μm diameter wire electrode. The work material was through-hardened AISI 52100 steel. Deionized water was the dielectric fluid supplied by controlled dripping into the EDM region.

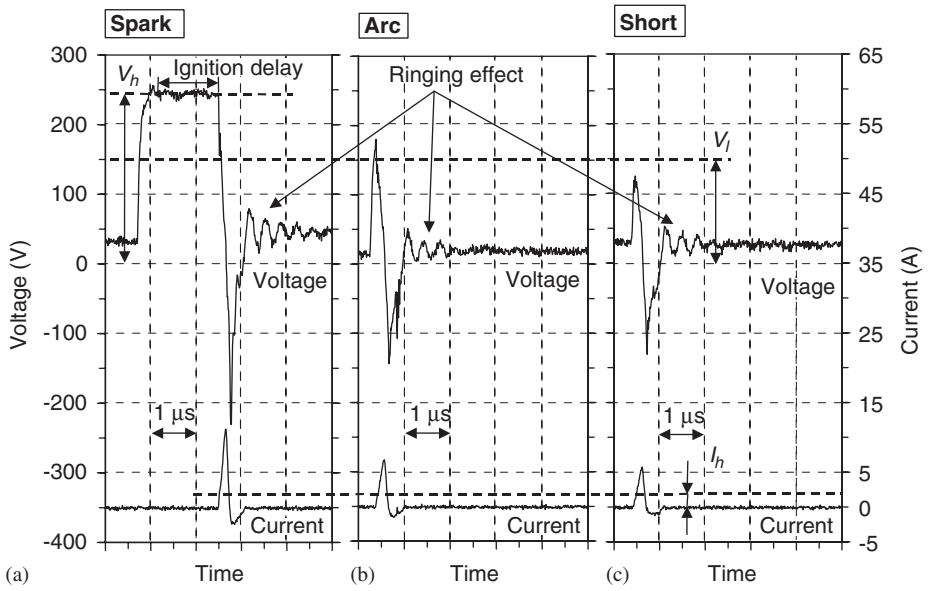

Fig. 3. Characterization of EDM pulses: (a) spark, (b) arc, and (c) short.

2.2. Data acquisition and classification of EDM pulses

An Agilent Infiniium 54833A digital oscilloscope with 2 GHz sampling rate was used for real-time acquisition of the gap voltage and current during micro-hole EDM. This dual-channel oscilloscope was equipped with an Agilent 10076A 250 MHz 100:1 high-voltage probe and an Agilent 1147A 50 MHz AC/DC current probe.

The highest sampling rate (2 GHz) was utilized to observe details of the rapidly changing voltage and current of spark, arc, and short pulses in micro-hole EDM. At a reduced sampling rate of 10 MHz, pulse trains of 3 ms (30,000 data points) were recorded every 4 s throughout the micro-hole drilling to study the rate of spark, arc, and short pulses. At least seven sets of 3 ms data were recorded for each micro-hole. Each data set was analyzed to identify and compare the rate of pulses under different EDM setups.

Algorithms developed by Dauw et al. [14] were applied to classify measured voltage and current behavior as either spark, short, or arc pulses based on preset voltage and current threshold values. Although more advanced EDM pulse classification methods such as the data dependent system [15], artificial intelligence [16–19], and wavelet transform [20] are available, the simple method based on Dauw et al. [14] is efficient and adequate. The spark, arc, and short pulses are identified in EDM pulse trains based on the high and low threshold voltages, V_h and V_l, respectively, and the threshold current I_h, as shown in Fig. 3. A spark has a long ignition delay, which is marked in Fig. 3, and the voltage is above V_h before discharging. An arc has no ignition delay because the deionization from the previous pulse is not complete and the remnant plasma channel has a residual conductivity that provides a passage for electric current to flow through [3]. The peak voltage in an arc is between V_h and V_l. For a short pulse, the contact between the electrode and workpiece causes a high current peak above I_h, and the gap voltage is below V_l. A Matlab program was developed to process the data and automatically count and identify each EDM pulse. The rate of EDM pulses can also be calculated.

2.3. Input parameters and stages in micro-hole EDM

Five input or setup parameters are varied in the micro-hole EDM experiments.

- *Polarity*: Polarity is the pole designation of the workpiece and electrode. As shown in Fig. 1, positive polarity sets the workpiece as the anode and the electrode as the cathode, and vice versa for negative polarity. The choice of polarity can greatly affect the wear of wire electrodes. Electrode wear is expected to be high under negative polarity [7]. This property is used to blunt the tip of the electrode, a procedure known as electrode dressing. During drilling, to reduce the electrode wear, positive polarity was used.
- *Drilling depth*: The drilling depth, marked as D in Fig. 1, is the travel of the wire electrode from the initial contact with the workpiece. The drilling depth is controlled by the servo motor and affected by the electrode wear.
- *Open circuit voltage*, V_o: This is the system voltage when the EDM circuit is in the open state and energy has been built up for discharging. An example of an open circuit voltage of 210 V is shown in Fig. 4.
- *Pulse duration time*, T_D: As shown in Fig. 4, T_D is the time duration of the positive discharging current in a single EDM pulse. The measured value of T_D is usually longer than the input value because of the time required for the current to rise and fall during discharging. The input value for T_D of the spark in Fig. 4 was 0.1 μs. The actual value was about 0.3 μs.

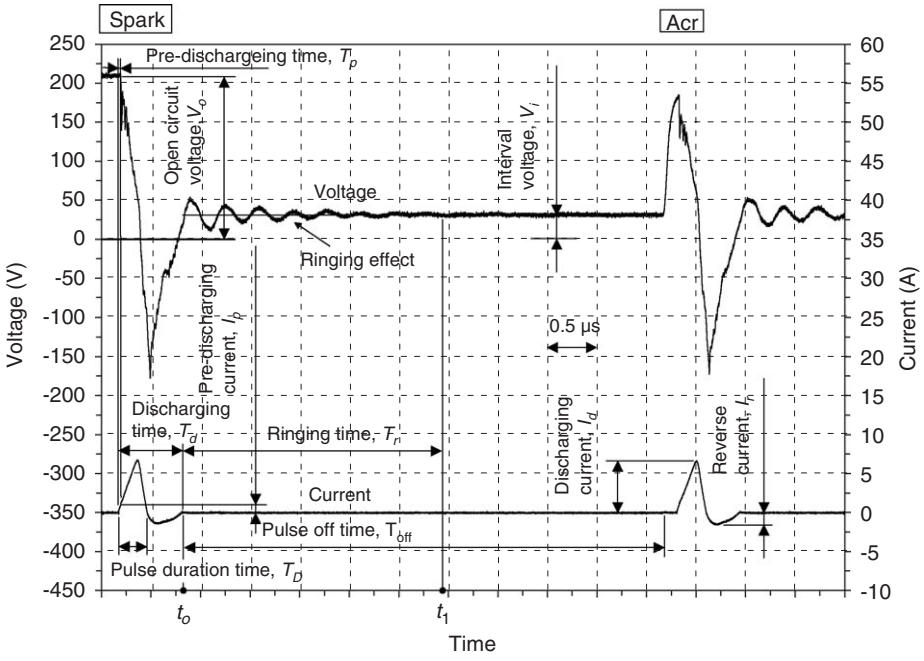

Fig. 4. EDM process input and output parameters of sample spark and arc pulses.

Table 1
Input parameters of micro-hole EDM

Stage	1	2	3
Function	Electrode dressing	Drilling	Penetration
Open circuit voltage, V_o (V)	170	210	240
Level of pulse energy	Low	Medium	High
Polarity	Negative	Positive	Positive
Drilling depth (mm)	0.10	0.76	1.20
Electrode travel relative to the hole depth (%)	11	73	16

- *Pulse off time*, T_{off}: This is the time from the end of one EDM pulse to the beginning of the next pulse, as shown in Fig. 4. During the pulse off time, the pulse generator is in the off state and the current is zero.

The EDM process used to drill a micro-hole suitable for a diesel engine injector is composed of three stages: electrode dressing, drilling, and penetration. Each stage, controlled by the drilling depth (without considering electrode wear) has its purpose. The settings of EDM parameters for all three stages are summarized in Table 1.

- *Stage* 1. *Electrode dressing*: The tip of the tungsten wire electrode is sharpened during this micro-hole EDM process. Fig. 5(a) shows an example of the sharpened electrode tip after completing EDM drilling of a 0.9 mm deep hole. The electrode dressing stage is implemented at the beginning of contact between the electrode and workpiece by using negative polarity to increase the electrode wear and blunt the tip. This has been proven to be important to maintaining the consistency of the micro-hole diameter in practical applications. The open circuit voltage V_o in Stage 1 is low (170 V), compared to other two stages. A low V_o can reduce debris size under negative polarity. The electrode travel in Stage 1 is short, only 0.1 mm. Fig. 5(b) shows the shape of an electrode tip after Stage 1. The electrode tip is blunted and covered by a thin recast layer.
- *Stage* 2. *Drilling*: Positive polarity and medium V_o (210 V) were applied in Stage 2 to increase the drilling speed while maintaining reasonable debris size for efficient flushing. This stage accounts for 0.66 mm or 73% of the electrode travel relative to the hole depth.
- *Stage* 3. *Penetration*: As shown in Fig. 6(a), at the time when the sharp electrode tip penetrates the other face of the workpiece, the electrode still needs to move forward by a set distance, called the over-travel, to maintain a consistent diameter inside the hole. From the diesel engine emissions perspective, a larger hole diameter in the final penetration stage, as shown in Fig. 6(b), is preferred. This is achieved by using a high V_o (240 V) and positive polarity, which increases the gap distance and rounds the fuel inlet edge in the micro-hole.

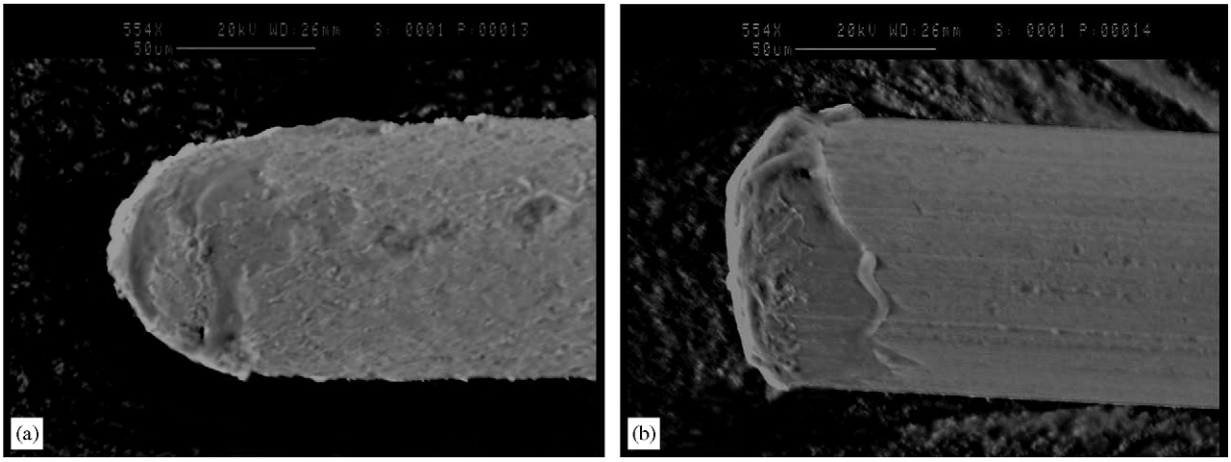

Fig. 5. SEM micrographs of the tip of tungsten wire electrode: (a) sharpened electrode tip after EDM Stage 3 and (b) dressed electrode tip after EDM Stage 1 (diameter of wire electrode: 125 μm).

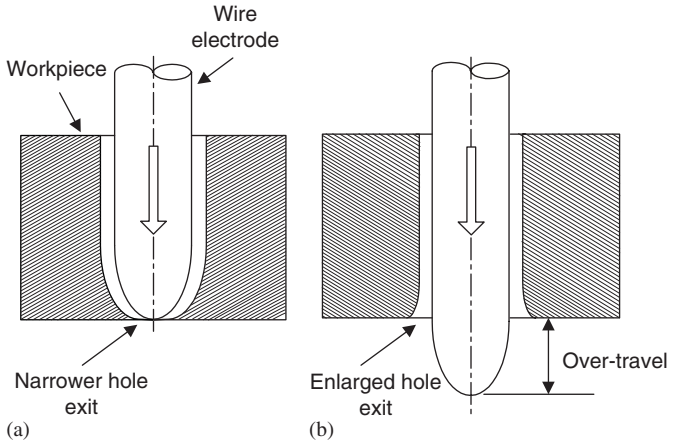

Fig. 6. The effect of EDM Stage 3 penetration: (a) worn tip of wire electrode causes a narrower hole exit and (b) enlarged hole exit is generated due to the over-travel of wire electrode.

The T_D and T_{off} were set at 0.1 and 5 μs, respectively, for all three stages.

The depth of hole was 0.9 mm. The setup for Stage 1 was used for the first 0.1 mm of electrode travel after the initial contact with the workpiece. Due to electrode wear, the actual depth of the hole drilled in Stage 1 was shorter than 0.1 mm. At 0.1 and 0.76 mm drilling depth (D), the EDM setup was changed to Stages 2 and 3, respectively. The EDM process stopped at 1.2 mm drilling depth, which had 0.3 mm of over-travel.

2.4. EDM output parameters

Seven EDM output parameters were measured for monitoring of EDM pulses. All seven parameters are marked in Fig. 4.

- *Discharging current*, I_d: This is the peak positive current during discharging.
- *Reverse current*, I_r: This is the peak negative current during discharging. The reverse current, which has been reported by Hebbar [3], flows opposite to the discharging current due to the parasitic capacitance of the system [2,11].
- *Pre-discharging current*, I_p: Using the 2 GHz sampling rate, a unique phenomenon was discovered in this study. The current starts to increase before the drop of voltage in discharging. The peak current before the voltage drop is defined as the pre-discharging current.
- *Pre-discharging time*, T_p: The time duration from the increase of current to the voltage drop in the beginning of discharging is defined as the pre-discharging time, T_p.
- *Discharging time*, T_d: This is the time duration that the discharging current, both positive and negative, exists.
- *Interval voltage*, V_i: This is the steady-state voltage after the ringing dissipates. The interval voltage is not constant for all pulses in an EDM pulse train. The value depends on the gap conditions, such as purity of dieletric fluid and concentration of debris.
- *Ringing time*, T_r: Analogous to the definition of settling time in the transient response analysis of dynamic systems [21], the ringing time is defined as the time duration from t_o, the instance when the negative current increases to zero, to t_1, when the voltage oscillation reaches and stays within the range of the 5% of the interval voltage V_i. Both t_0 and t_1 are marked in Fig. 4.

3. EDM pulses

Using a 0.5 ns sampling interval, the representative spark and arc of Stages 2, 1, and 3 are presented in Figs. 7, 9, and 10, respectively. Six successive periods, denoted as Period I–VI, are identified in each sample spark and arc pulse.

- *Period* I: The voltage rises and stays at a specified open circuit voltage V_o while the current remains zero. In

Period I, the wire electrode is gradually approaching the workpiece.

- *Period* II: The current rises and voltage remains the same in this period. The pre-discharging current I_p occurs at the end of Period II. The time duration of Period II is the pre-discharging time T_p. In Period II, the parasitic capacitance [2], which is inherent in the EDM circuit, begins to be charged.
- *Period* III: The voltage drops from the open circuit voltage V_o to zero in this period. In the beginning of Period III, a very rapid voltage drop occurs. The rate of voltage drop will be analyzed in Section 3.1. A high-frequency voltage oscillation due to the fast change of the gap impedance [22] occurs following the rapid voltage drop. The current typically rises to a peak value in Period III.
- *Period* IV: Period IV begins at the zero voltage and ends when the current reaches zero. The voltage becomes negative in this period.
- *Period* V: This is the period with the negative reverse current and its peak value I_r occur.
- *Period* VI: This is the ringing period.

3.1. Spark and arc pulses in Stage 2 (drilling)

A spark pulse from Stage 2, as is illustrated in Fig. 7(a), is more representative and, hence, discussed first. In Period I, the open circuit voltage V_o is 210 V and the current

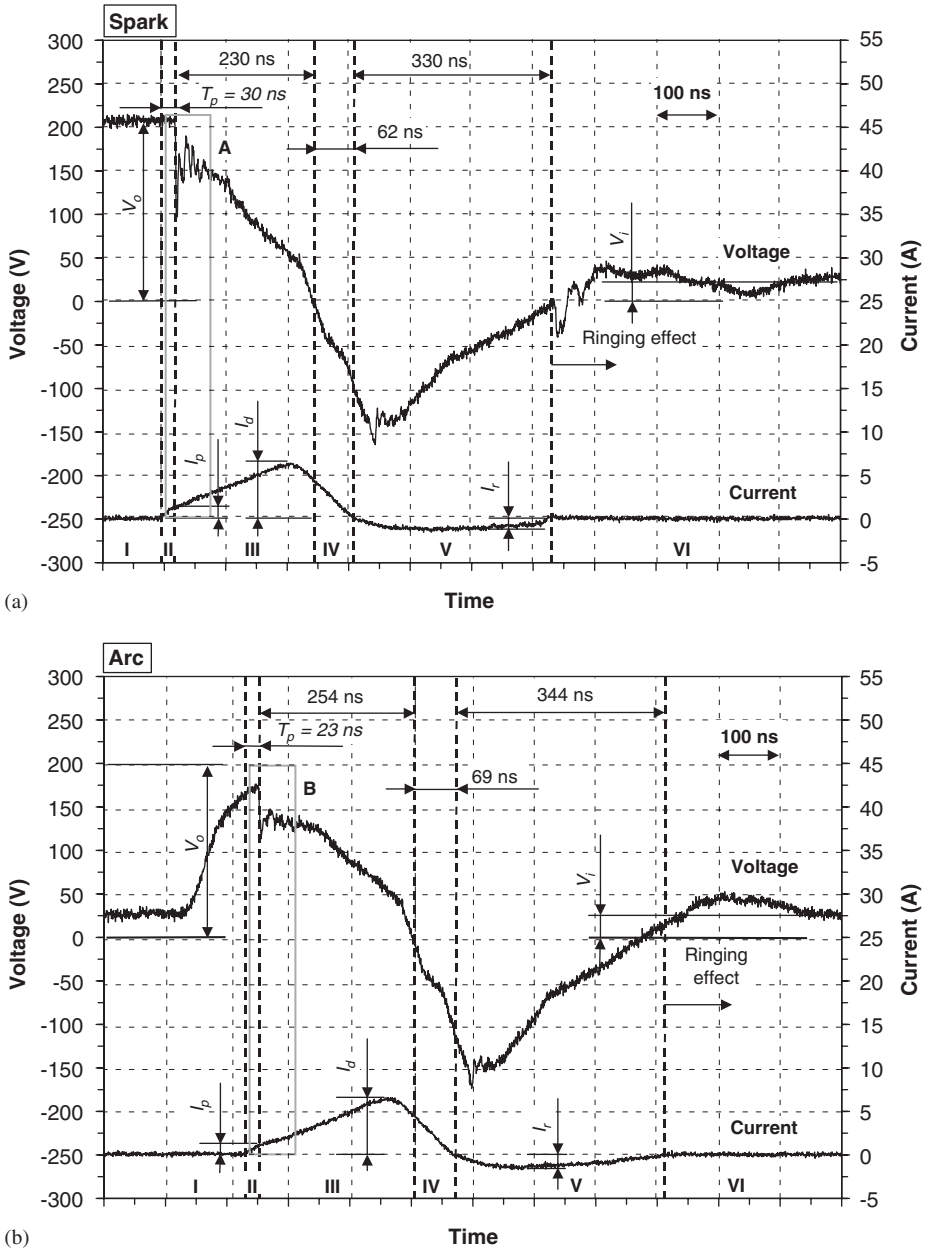

Fig. 7. Sample EDM pulses in Stage 2: (a) spark and (b) arc (125 μm diameter wire electrode).

is zero. The pre-discharging time T_p is 30 ns and the pre-discharging current I_p is 1.1 A in Period II. A close-up view of the voltage drop, as marked by box A in Fig. 7(a), is shown in detail in Fig. 8(a). The rate of voltage drop is −37.6 V/ns. In Period III, the discharging current I_d is 6.3 A and the time duration is 230 ns. In Period V, the reverse current I_r reaches −1.2 A. The discharging time T_d, which is the time duration from Period II–V, is 652 ns. The interval voltage V_i is estimated to be 28 V in Period VI.

An arc pulse from Stage 2 is shown in Fig. 7(b). In Period I, the voltage gradually rises but does not stay at the V_o before the discharging. In Period II, the duration T_p is 23 ns and I_p is 1.2 A. In Period III, the rapid voltage drop begins at 172 V, which is 38 V lower than the V_o. The close-up view of the voltage drop, as marked by box B in Fig. 7(b), is shown in Fig. 8(b). The rate of voltage drop is −14.7 V/ns, which is lower than that in the spark pulse. Hebbar [3] has proposed to use the rate of voltage drop at discharge to differentiate between the spark and arc pulses. In Period III, the amplitude of the high-frequency voltage oscillation can also be seen. The current I_d is 6.5 A in Period III. The duration of Period IV is 69 ns. In Period V, the I_r is −1.5 A and the duration is 344 ns. The T_d is 690 ns, about 6% longer than that of the spark pulse. The interval voltage V_i is estimated as 25 V in Period VI. In general, the duration of pre-discharging, the voltage at discharge, and the rate of voltage drop at the beginning of discharging are all lower in an arc than those in a spark.

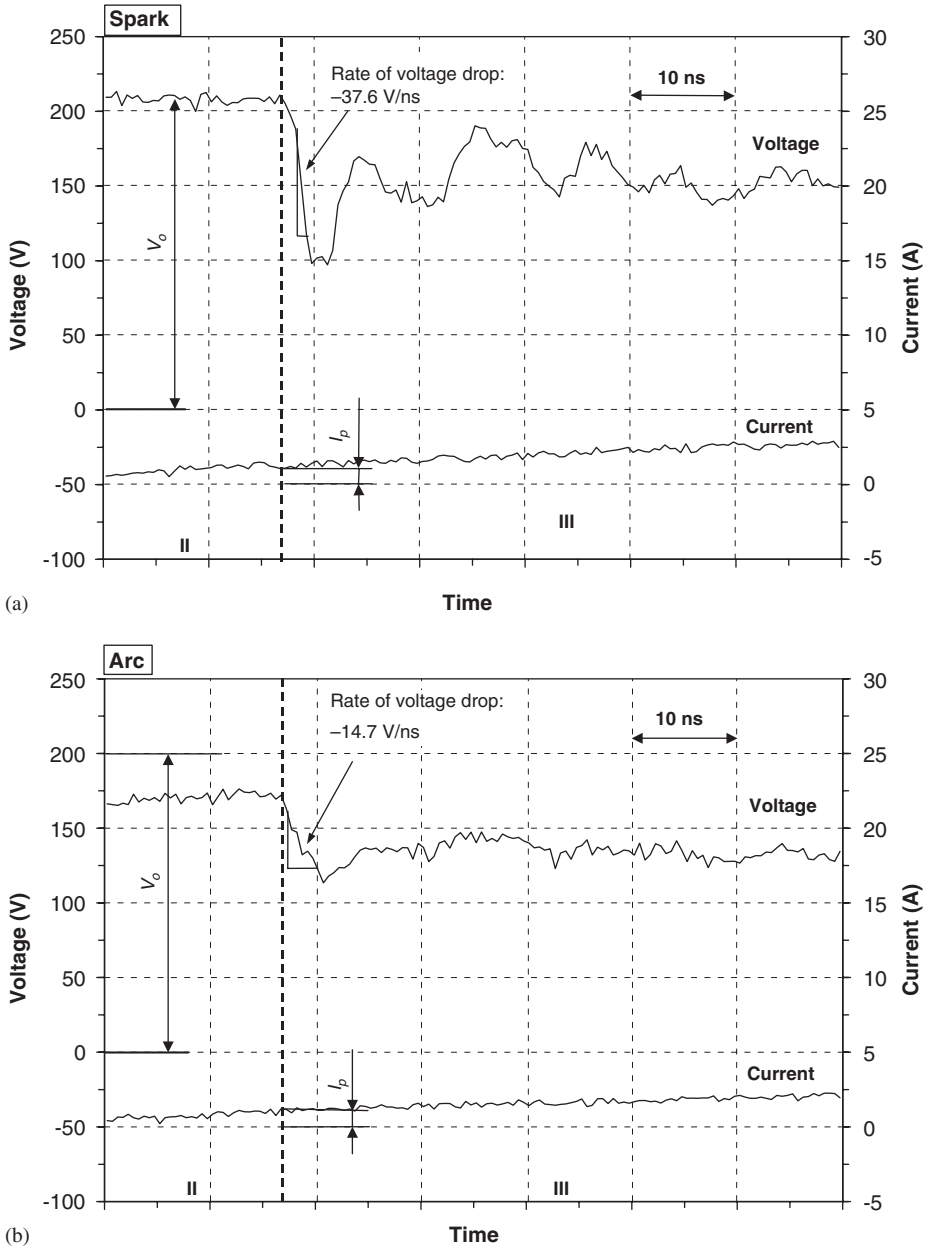

Fig. 8. Close-up view for Periods II and III of sample EDM pulses in Stage 2: (a) box A and (b) box B.

3.2. Spark and arc pulses in Stage 3 (penetration)

A spark pulse in Stage 3 is shown in Fig. 9(a). In Period I, the open circuit voltage V_o is 240 V, and the current is zero. In Period II, the pre-discharging time T_p is 25 ns and pre-discharging current I_p is 1.6 A. In Period III, the voltage drops quickly, at a rate of −51.7 V/ns. The discharging current I_d is high, 7.6 A. In Period V, the reverse current I_r is −1.6 A, also higher than that of the spark in Stage 2. The discharging time T_d is 646 ns, about the same as that of a spark in Stage 1. In Period VI, the interval voltage V_i is 43 V, higher than that of the spark in Stage 2.

An arc pulse in Stage 3 is shown in Fig. 9(b). A gradual voltage increase occurs in Periods I and II. The peak voltage is 220 V, 20 V lower than the specified V_o, at the end of Period II when the voltage starts to drop. In Period II, the $T_p = 28$ ns and $I_p = 1.4$ A. The rate of voltage drop is −20.9 V/ns, which is lower than that in spark in Stages 2 and 3. In Period III, the I_d is high, 7.9 A. The I_r in Period V is −1.7 A. The T_d is 668 ns, slightly longer than that of the spark pulse in Stage 3. The interval voltage V_i was estimated as 35 V in Period VI.

3.3. Spark and arc pulses in Stage 1 (electrode dressing)

The negative polarity setup changes the shape of the waveform for both spark and arc pulses in Stage 1. A spark pulse is shown in Fig. 10(a). To make the shape consistent for comparison, the measured signal was multiplied by −1.

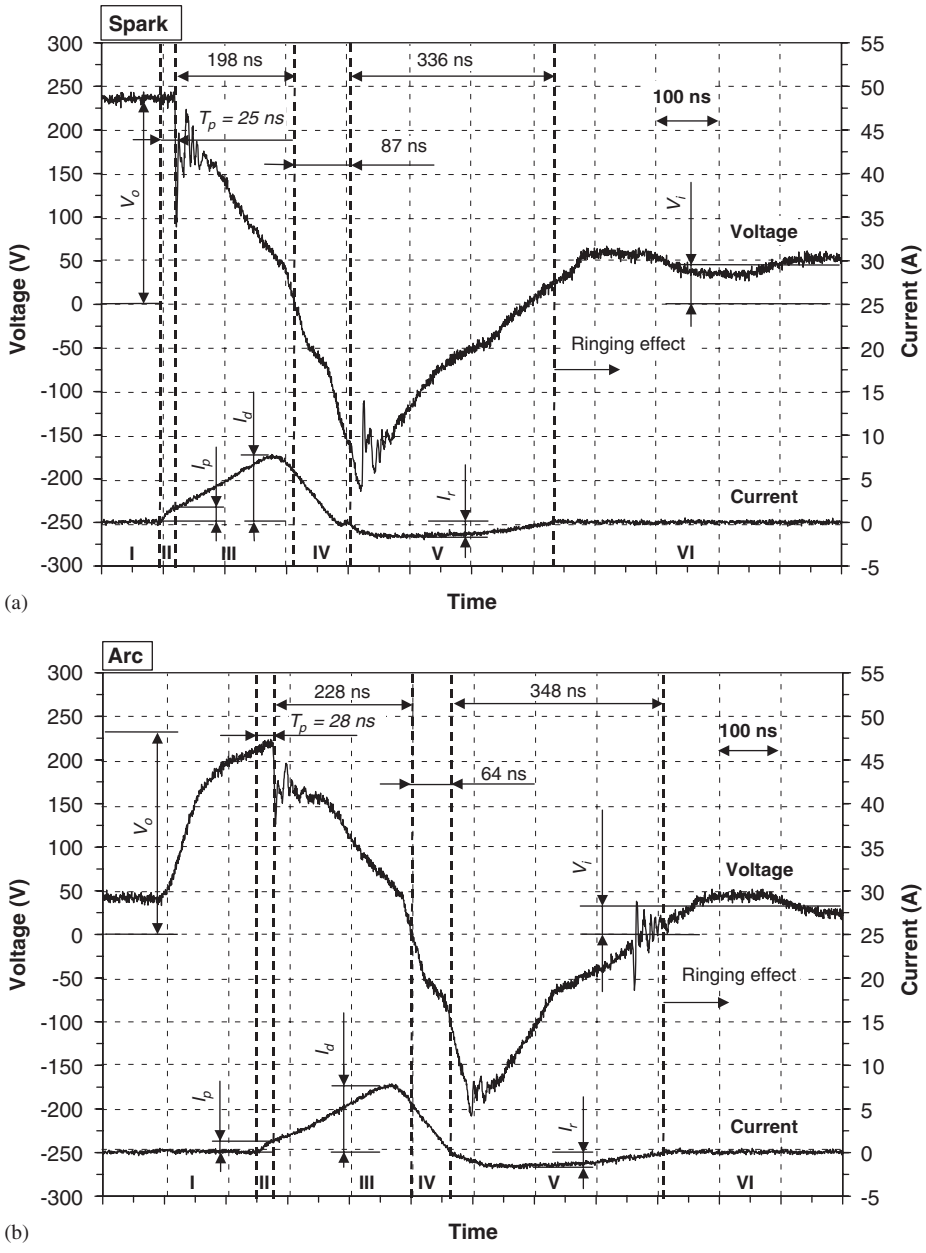

Fig. 9. Sample EDM pulses in Stage 3: (a) spark and (b) arc (125 μm diameter wire electrode).

The voltage V_o is low, 170 V. The output parameters in Periods II and III are about the same as the spark in Stages 1 and 3: $T_p = 30$ ns, $I_p = 1.1$ A, $I_d = 8.3$ A, and rate of voltage drop is -20.5 V/ns.

The most significant impact of negative polarity occurs after the voltage drops below zero. Instead of continuing to reduce to -150 V in Stage 2 (Fig. 7) or -200 V in Stage 3 (Fig. 9), the voltage reduces to only -70 V, marked by circle C in Fig. 10(a), and starts to increase. The gradually increasing voltage results in a lower rate of current drop and elongates the time duration of Period IV, from less than 90 ns under positive polarity to 240 ns using the negative polarity. The effect of a polarity change on electrode wear has been studied [7]. The small debris generated is likely to be negatively charged and accelerate to impact and neutralize the positive charged tungsten electrode. This reduces the level of voltage below zero. The reverse current I_r is -1.7 A in Period V. The discharging time T_d is long, 1372 ns, more than twice of that in Stages 2 and 3. In Period VI, the interval voltage V_i is very low, only 8 V.

An arc pulse in Stage 1 is shown in Fig. 10(b). Two peaks of current are recognized. The voltage rises to about 70 V in the end of Period II. Both I_p (0.2 A) and T_p (16 ns) are very small. Although the initial voltage drop in Period III was slow, only -0.6 V/ns, the voltage drops quickly to zero. Period III is also short, only 125 ns. The peak current does not happen in Period III as in other arc and spark pulses in Stages 2 and 3. In Period IV, the current reaches its first peak (2.0 A), marked as I_{d1}, as the voltage continues

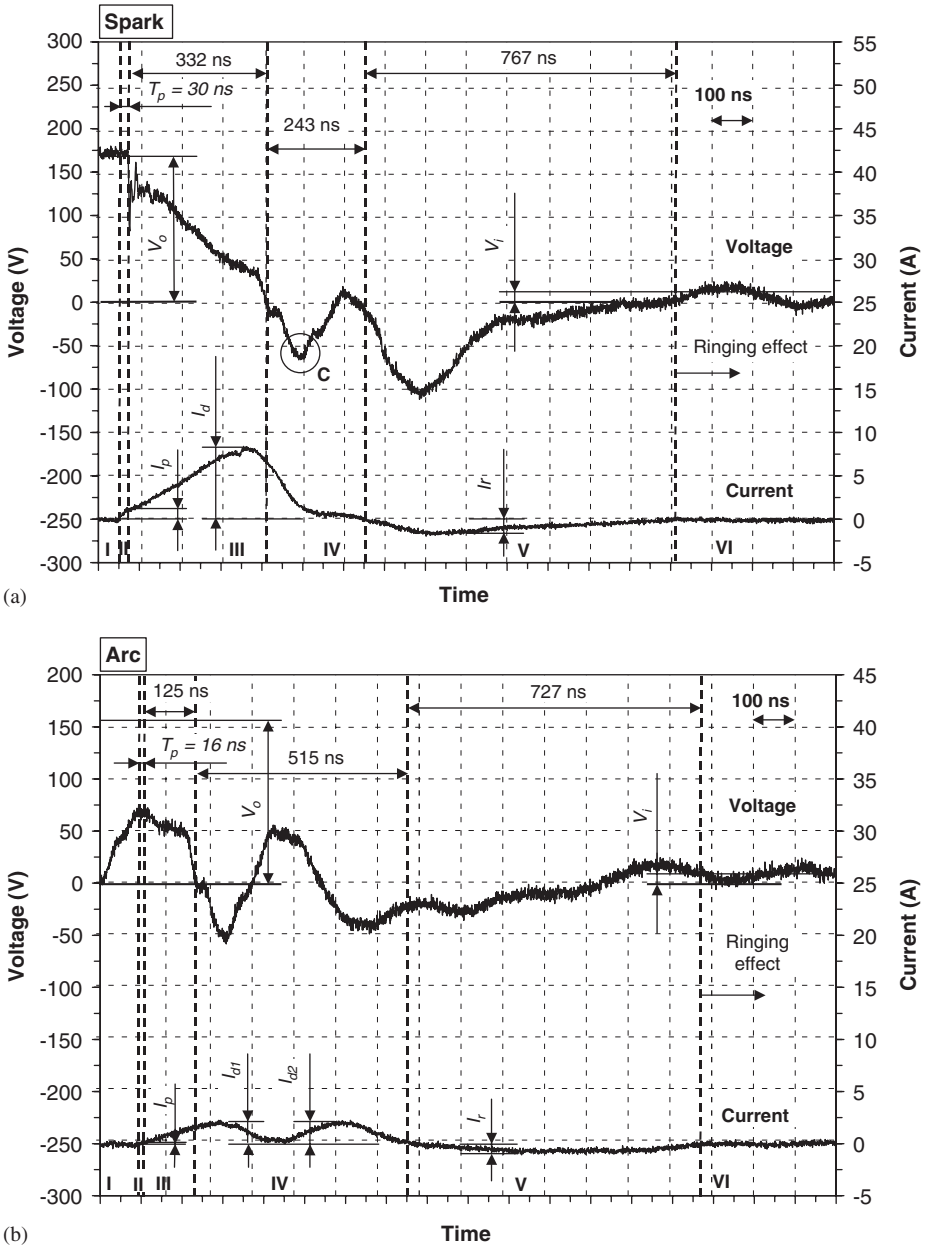

Fig. 10. Sample EDM pulses in Stage 1: (a) spark and (b) arc (125 μm diameter wire electrode).

to drop. After the first peak in current, the voltage rises to 50 V in 120 ns and starts another discharge. The magnitude of second discharging current, denoted I_{d2}, is also about 2.0 A. The period of reverse current, Period V, still exists and I_r (−0.8 A) is very small. The time duration for an arc pulse with two discharges (T_d) is 1383 ns, about the same as that of the spark pulse in Stage I. In Period VI, the V_i is low, about 10 V.

4. Pulse rate and electrode feed rate

The rate of spark, arc, and short pulses in Stages 1–3 for 125 and 225 μm diameter wire electrodes are analyzed and the results are shown in Fig. 11.

In Stage 1, due to the negative polarity setting used to increase electrode wear, high short pulse rate and low spark pulse rate are observed. The lack of spark pulses and frequent short pulses affect the efficiency of removing the work-material. The electrode feed rate is the slowest in Stage 1, as shown in Fig. 12. The diameter of electrode wire has an effect on the feed rate. Although the 225 μm electrode has more frequent spark pulses and less frequent short pulses than that of the 125 μm electrode, as shown in Fig. 12, the electrode feed rate is slightly faster for the 125 μm electrode. This is due to the fact that less volume of work material is removed by the 125 μm electrode during EDM. Debris flushing was not a problem for 125 mm electrode.

In Stage 2, as shown in Fig. 11, the pulse rate for sparking is much higher than in Stage 1. The EDM process was adjusted to achieve a high spark pulse rate in this stage for fast material removal. The electrode feed rate, as shown in Fig. 12, has increased to 2.8 and 2.6 mm/min for 125 and 225 μm electrode, respectively. Similar to Stage 1, the 225 μm electrode has more frequent spark pulses but a slower feed rate than the 125 μm electrode.

In Stage 3, the high V_o slightly reduces the spark pulse rate but significantly increases the electrode feed rate, particularly for the 125 μm electrode. Each spark pulse under high V_o has more energy, which removes more work material and increases the gap width. This is important to create the desired reverse taper shape of spray hole with larger diameter inside the hole. Although a high V_o is helpful to increasing the electrode feed rate to 6.7 and 4.5 mm/min for 125 and 225 μm diameter wire, respectively, it deteriorates the roundness of the hole. All of these have been observed in a study to measure the form of the spray hole under the same EDM setup in this paper [23].

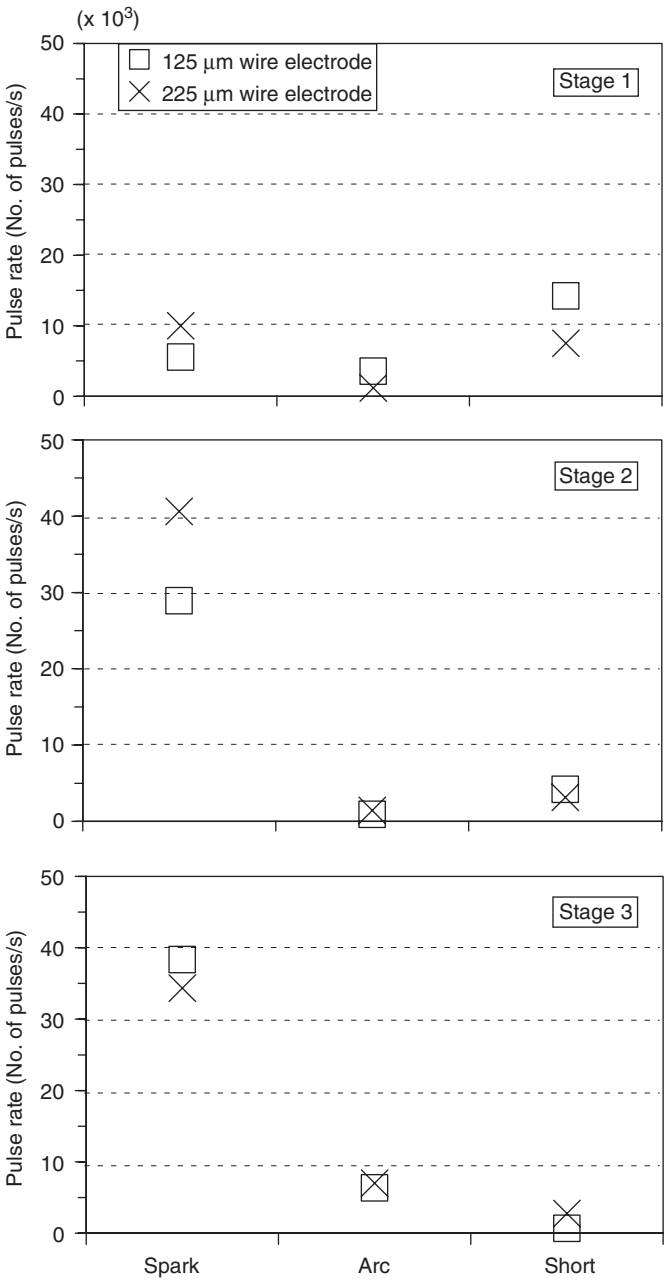

Fig. 11. Rate of spark, arc, and short pulses for 125 and 225 μm wire electrodes in three EDM stages.

5. Ringing model

Due to the parasitic inductance and capacitance inherent in the electronic circuit under high-speed switching in micro-hole EDM, the oscillation (or ringing) of decaying gap voltage at the end of each spark and arc pulse is inevitable [11]. For micro-hole EDM, as shown in the sample spark and arc pulses in Fig. 4, the ringing of gap voltage occupies over 60% of pulse off time. Modeling the oscillation of gap voltage can help give a better understanding of the ringing effect and lead to more efficient EDM circuit design and process parameter selection.

5.1. Modeling of voltage oscillation after discharging

A RLC circuit model, as shown in Fig. 13, was developed. Parameters used in this model are: gap voltage V_g, parasitic resistance R_p, parasitic capacitance C_p, parasitic inductance of electrode L_e, parasitic inductance of the jumper cable for the voltage probe L_p, and a DC

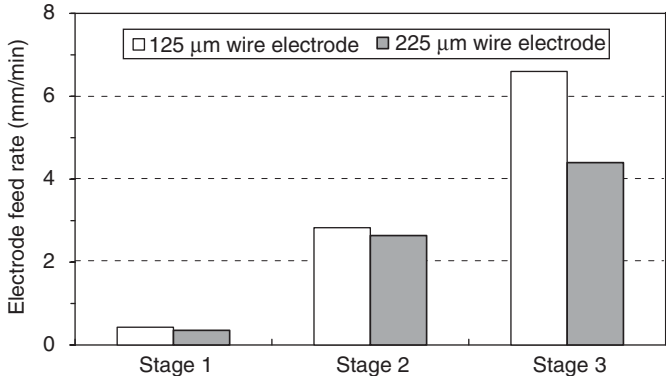

Fig. 12. Feed rate for 125 and 225 μm wire electrodes in three EDM stages.

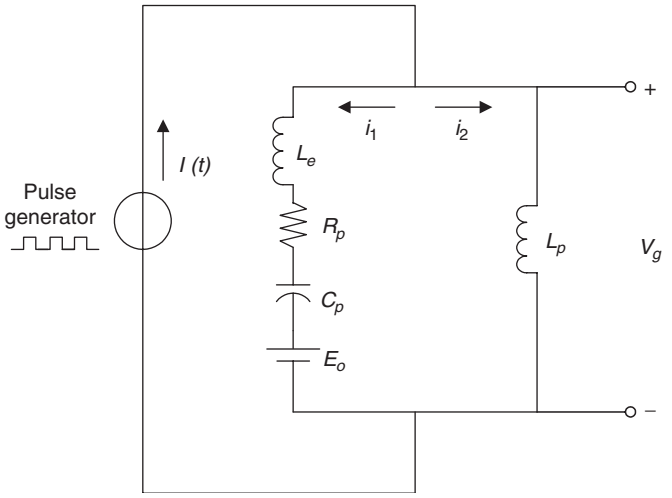

Fig. 13. A RLC circuit for the modeling of ringing effect.

voltage source representing the open-circuit voltage across discharge gap E_o [2]. A schematic diagram of each component of the circuit corresponding in the EDM setup and the arrangement of voltage probe and jumper cable are illustrated in Fig. 14. Values of L_e and L_p can be estimated by [24]

$$L = 0.002l\left[\ln\frac{2l}{\rho} - \frac{3}{4}\right], \tag{1}$$

where ρ is the wire radius in cm, l is the wire length in cm, and the unit of L is μH.

The second-order differential equation of the RLC circuit shown in Fig. 13 is

$$\frac{d^2V_g}{dt^2} + \frac{R_p}{L_e + L_p}\frac{dV_g}{dt} + \frac{1}{(L_e + L_p)C_p}V_g = 0. \tag{2}$$

Eq. (2) can be rewritten as

$$\frac{d^2V_g}{dt^2} + 2\xi\omega_n\frac{dV_g}{dt} + \omega_n^2 V_g = 0, \tag{3}$$

where $\xi = R_p/2\omega_n(L_e + L_p)$ is the damping ratio and $\omega_n = \sqrt{1/(L_e + L_p)C_p}$ is the resonant frequency of the EDM

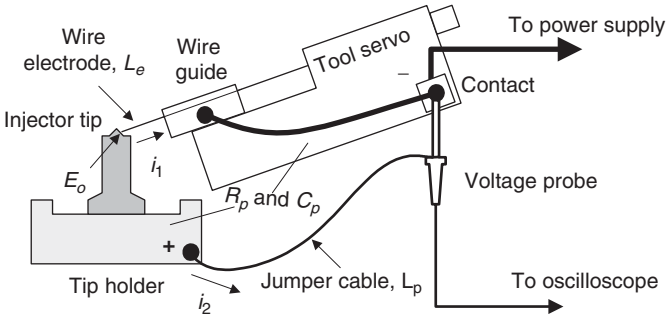

Fig. 14. Schematic diagram of the micro-hole EDM setup.

circuit. The homogenous solution of Eq. (3) is [25]

$$V_g = Ae^{-\xi\omega_n t}\sin(\omega_d t + \phi), \tag{4}$$

where A is the amplitude of voltage oscillation, called the ringing amplitude, $\omega_d(=\omega_n\sqrt{1-\xi^2})$ is the damped frequency, and ϕ is the phase shift.

In this study, the ringing oscillates from negative voltage to zero. The envelope curve to represent the oscillating decay is given by

$$V_g = -Ae^{-\xi\omega_n t}. \tag{5}$$

The ξ and ω_n are solved by processing the data of gap voltage V_g vs. time t in the ringing region. The decay rate $\xi\omega_n$ and period of decay oscillation T are identified from the six data points, as marked in Fig. 15, in Period VI. Three examples of the ringing of spark pulses in Stage 2 using 100, 125, and 225 μm diameter wire electrodes are shown in Fig. 15 to demonstrate the data processing procedure. The $t = 0$ is defined at the end of Period V when the current is zero. The first data point is located at $t = 0$. The following five peaks in Period VI are identified. The average of three time spans between adjacent peaks 2, 3, 4, and 5 is used to represent the period T. Fitting the six data points using Eq. (4), the decay rate $\xi\omega_n$ can be determined. It is important to note that the 0.5 ns high-speed data acquisition is crucial to accurately determine T and $\xi\omega_n$. Knowing $T(=2\pi/\omega_d)$, $\xi\omega_n$, L_e, and L_p, the values of C_p and R_p are obtained from Eqs. (6) and (7).

$$C_p = \frac{1}{(L_e + L_p)\omega_n^2}, \tag{6}$$

$$R_p = 2\xi\omega_n(L_e + L_p). \tag{7}$$

These two variables are intrinsic system parameters and should not change under different EDM setups. Two sets of experiments, one varying wire electrode diameter and the other changing open circuit voltage, are conducted to test the variation of C_p and R_p to validate the proposed RLC circuit for ringing model.

5.2. Influence of the electrode size

The spark pulse in Stage 2 of 100, 125, and 225 μm diameter electrodes, as shown in Fig. 15, are used to find

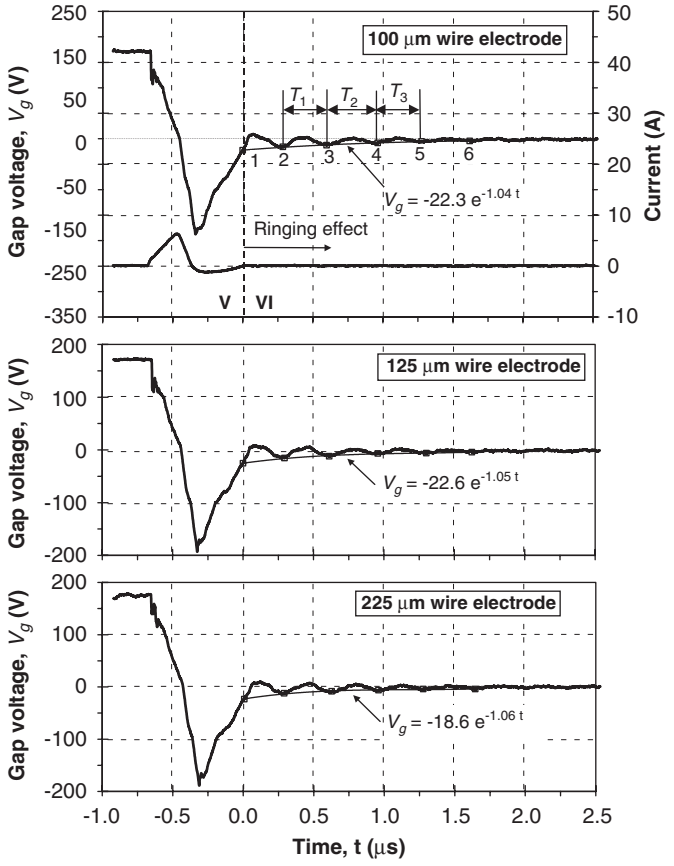

Fig. 15. Envelope curves of the ringing effect for 100, 125, and 225 μm diameter wire electrodes. ($V_o = 200$ V)

the C_p and R_p. Using Eq. (1), the parasitic inductance $L_p = 0.288\,\mu H$ ($l = 25$ cm and $\rho = 0.075$ cm) and $L_e = 0.069$, 0.066, and 0.060 μH for $l = 5$ cm and $\rho = 0.005$, 0.0063, and 0.011 cm, respectively.

For the 100, 125, and 225 μm diameter wire electrodes, $T = 0.33$, 0.32, and 0.32 μs and $\xi\omega_n = 1.04$, 1.05, and 1.06 s^{-1}, respectively. The ringing time T_r is about 2.3 μs for three wire electrodes. Results of the parasitic capacitance C_p and parasitic resistance R_p are listed in Table 2. Both C_p and R_p are almost the same for all three electrode diameters. This confirms the proposed ringing model.

5.3. Influence of the open circuit voltage

The open circuit voltage vs. time data in five experiments at 160, 180, 200, 230, and 250 V open circuit voltage is used to find the variation of C_p and R_p. The electrode diameter is 125 μm, the parasitic inductances $L_p = 0.288\,\mu H$ and $L_e = 0.066\,\mu H$. The ringing time T_r is about 2.3 μs for the five voltage setups. As listed in Table 3, C_p varies from 7.3 to 7.6 nF and R_p ranges from 0.687 to 0.828 Ω. The variation of C_p is small, while a reasonable variation of R_p, which increases with open circuit voltage, exists. A possible cause for the variation of R_p is the resistance variation across the discharge gap due to different levels of open circuit voltage. The ringing effect occurs at the end of discharging, while the heat-induced explosion destroys the plasma channel and generates a cavity within the dielectric fluid. A higher open circuit voltage corresponds to a higher pulse energy level and generates a stronger explosion, which cleans away the previous plasma channel more completely. This will reduce the concentration of remnant ions and electrons within the discharge gap and result in a higher resistance.

Table 2
Parasitic properties C_p and R_p with different electrode size ($V_o = 200$ V, $L_p = 0.288\,\mu H$)

Electrode diameter (μm)	100	125	225
L_e (μH)	0.069	0.066	0.060
Parasitic capacitance C_p (nF)	7.61	7.35	7.62
Parasitic resistance R_p (Ω)	0.743	0.743	0.738

Table 3
Parasitic properties C_p and R_p with different open circuit voltage V_o (diameter of wire electrode = 125 μm, parasitic inductance $L_e = 0.066\,\mu H$, and $L_p = 0.288\,\mu H$)

Open circuit voltage V_o (V)	160	180	200	230	250
Parasitic capacitance C_p (nF)	7.51	7.60	7.36	7.64	7.32
Parasitic resistance R_p (Ω)	0.687	0.729	0.743	0.807	0.828

6. Conclusions

In this study, a high-speed oscilloscope with 0.5 ns sampling period was applied to investigate spark and arc pulses for a better understanding of the micro discharging process. Sample spark and arc pulses for three stages (electrode dressing, drilling, and penetration) of micro-hole EDM were analyzed.

A new phenomenon of pre-discharging current, a short-time duration (less than 30 ns) current rise before the rapid voltage drop, was observed. The effect of electrode dressing using negative polarity was evidenced by SEM micrographs showing a blunted electrode tip. Negative polarity not only induced a high short pulse rate and elongated the discharging period, but also resulted in double discharges in arc pulses. When a wire electrode with larger diameter was used, a higher spark pulse rate was observed but it did not correspond to a high electrode feed rate.

A RLC circuit was proposed to model the ringing effect generated at the end of discharge. The inductance of the voltage probe jumper cable and the wire electrode was calculated and two parameters, parasitic capacitance C_p and resistance R_p, of the RLC circuit were calculated from the measured decaying voltage waveforms. Results showed that the proposed RLC circuit could model the ringing phenomenon, the electrode diameter had negligible effect

on ringing, and high open voltage increased the parasitic resistance and improved the damping in ringing.

Monitoring of voltage and current can assist in the selection and optimization of micro-hole EDM process parameters. Moreover, with the detail demonstration of nanosecond level interactions between the gap voltage and current, the EDM research can move further, while combining the knowledge of plasma physics, to the theoretical field, such as the study of nano-scale discharging mechanisms. The modeling of ringing phenomenon can help understand the effects of key circuit components and, in the future, help to reduce the ringing time. A reduction of ringing time can increase the pulse frequency as well as the electrode feed rate. The future research will focus on the reduction of ringing and real-time diagnosis of micro-hole EDM process through online monitoring.

Acknowledgements

Assistance of John MacGregor and George Barbulescu of Ann Arbor Machine is greatly appreciated.

References

[1] T. Masuzawa, J. Tsukamoto, M. Fujino, Drilling of deep microholes by EDM, Annals of the CIRP 38 (1) (1989) 195–198.
[2] K. Takahata, Y.B. Gianchandani, Batch mode micro-electro-discharge machining, Journal of Microelectromechanical Systems 11 (2) (2002) 102–110.
[3] R.R. Hebbar, Micro-hole drilling by electrical discharge machining, Ph.D. Dissertation, Purdue University, 1992.
[4] H. Morita, S. Ohyama, N. Mohri, Electrical discharge device with direct drive method for thin wire electrode, SAE Technical Papers 2000-01-1085, 2000.
[5] T.V. Johnson, Diesel emission control in review—the last 12 months, SAE technical paper series 2003–01–0039, 2003.
[6] H. Nordgren, A. Hultqvist, B. Johansson, Start of injection strategies for HCCI-combustion, SAE technical paper series 2004–01–2990, 2004.
[7] M.G. Her, F.T. Weng, Micro-hole machining of copper using the electro-discharge machining process with a tungsten carbide electrode compared with a copper electrode, International Journal of Advanced Manufacturing Technology 17 (10) (2001) 715–719.
[8] B.H. Yan, F.Y. Huang, H.M. Chow, J.Y. Tsai, Micro-hole machining of carbide by electric discharge machining, Journal of Materials Processing Technology 87 (1–3) (1999) 139–145.
[9] J.S. Soni, G. Chakraverti, Machining characteristics of titanium with rotary electro-discharge machining, Wear 171 (1–2) (1994) 51–58.
[10] B. Mohan, A. Rajadurai, K.G. Satyanarayana, Electric discharge machining of Al-SiC metal matrix composites using rotary tube electrode, Journal of Materials Processing Technology 153–154 (1–3) (2004) 978–985.
[11] J.L. Kuo, Z.S. Chang, J.D. Lee, Y.C. Chio, P.H. Lee, Ringing effect analysis of the digital current pulse generator for the linear rail gun, IEEE Industry Applications Society Annual Meeting 1 (2002) 176–181.
[12] Y.S. Wong, M. Rahman, H.S. Lim, H. Han, N. Ravi, Investigation of micro-EDM material removal characteristics using single RC-pulse discharges, Journal of Materials Processing Technology 140 (1-3) (2003) 303–307.
[13] F. Han, S. Wachi, M. Kunieda, Improvement of machining characteristics of micro-EDM using transistor type isopulse generator and servo feed control, Precision Engineering 28 (2004) 378–385.
[14] D.F. Dauw, R. Snoeys, W. Dekeyser, Advanced pulse discriminating system for EDM process analysis and control, Annals of the CIRP 32 (2) (1983) 541–549.
[15] S.M. Pandit, T.M. Mueller, Verification of on-line computer control of EDM by data dependent systems, Journal of Engineering for Industry 109 (2) (1987) 117–121.
[16] K.H. Ho, S.T. Newman, State of the art electrical discharge machining (EDM), International Journal of Machine Tools and Manufacture 43 (13) (2003) 1287–1300.
[17] Y.S. Tarng, C.M. Tseng, L.K. Chung, A fuzzy pulse discriminating system for electrical discharge machining, International Journal of Machine Tools and Manufacture 37 (4) (1997) 511–522.
[18] J.Y. Kao, Y.S. Tarng, A neural-network approach for the on-line monitoring of the electrical discharge machining process, Journal of Materials Processing Technology 69 (1–3) (1997) 112–119.
[19] H.S. Liu, Y.S. Tarng, Monitoring of the electrical discharge machining process by abductive networks, International Journal of Advanced Manufacturing Technology 13 (4) (1997) 264–270.
[20] S.F. Yu, B.Y. Lee, W.S. Lin, Waveform monitoring of electric discharge machining by wavelet transform, International Journal of Advanced Manufacturing Technology 17 (5) (2001) 339–343.
[21] K. Ogata, Modern control engineering, fourth ed., Pearson Education Ltd., Singapore, 2004.
[22] S.K. Bhattacharyya, M.F. El-Menshawy, Identification of the discharge profile in E.D.M., in: Proceedings of the New England Bioengineering Conference, Gainesville, FL, USA, 1978, pp. 351–356.
[23] C.C. Kao, A.J. Shih, Form measurements of micro-holes, Precision Engineering, submitted for publication.
[24] F.W. Grover, Inductance Calculations, D. Van Nostrand Company, Inc., New York, 1946.
[25] D.J. Inman, Engineering Vibration, second ed., Prentice Hall, New Jersey, 2001.